Use of inverted echosounders to monitor the migration timing and abundance of juvenile salmon in the Discovery Islands, British Columbia

S. Rousseau, S. Gauthier, S. Johnson
C. Neville and M. Trudel

Fisheries and Oceans Canada
Science Branch, Pacific Region
9860 West Saanich Road
Sidney, BC, Canada
V8L 4B2

2017

Canadian Technical Report of Fisheries and Aquatic Sciences

Fisheries and Oceans Canada   Pêches et Océans Canada

Canada

Canadian Technical Report of
Fisheries and Aquatic Sciences

2017

USE OF INVERTED ECHOSOUNDERS TO MONITOR THE MIGRATION TIMING AND ABUNDANCE OF JUVENILE SALMON IN THE DISCOVERY ISLANDS, BRITISH COLUMBIA

By

S. Rousseau[1], S. Gauthier[1], S. Johnson[2]
C. Neville[2] and M. Trudel[3]

[1]Fisheries and Oceans Canada, Science Branch, Pacific Region, 9860 West Saanich Road, Sidney, BC, Canada, V8L 4B2

[2]Fisheries and Oceans Canada, Science Branch, Pacific Region, 3190 Hammond Road, Nanaimo, BC, Canada, V9T 6N7

[3]Fisheries and Oceans Canada, Science Branch, Atlantic Region, 531 Brandy Cove Road, St. Andrews, New Brunswick, Canada, E5B 2L9

Cat. No. Fs97-6/3227E-PDF IBSN 978-0-660-09542-4 ISSN 1488-5379

Correct citation for this publication:

Rousseau, S., Gauthier, S., Johnson, S., Neville, C. and Trudel M., 2017. Use of inverted echo-sounders to monitor the migration timing and abundance of juvenile salmon in the Discovery Islands, British Columbia. Can. Tech. Rep. Fish. Aquat. Sci. 3227: viii + 33 p.

Contents

List of Figures

List of Tables

Abstract

The purpose of this project was to evaluate the use of inverted echosounders to monitor juvenile salmon abundance, behaviour and migration timing in the Discovery Islands and Johnstone Strait area. Four inverted, single-beam echosounders were deployed in 2015 and five were deployed in 2016, collecting multi-frequency acoustic data from May to September. This report describes the methodology and primary results obtained from data collected at a site that was monitored in 2015 and 2016. This site is located in Okisollo channel, in the Discovery Islands. Juvenile salmon migration timing obtained acoustically is in good agreement with that observed by DFO's purse seine program. Peak migration occurred from mid-May to mid-July in 2015, and from mid-May to mid-June in 2016. Total abundances (all salmon species combined) were similar in 2015 and 2016. Mean school depth of juvenile salmon was 5.3 $\pm$ 1.7 m and 3.5 $\pm$ 1 m in 2015 and 2016, respectively, and school's vertical extent in the water column was 5.9 $\pm$ 0.9 m and 4.9 $\pm$ 1 m in 2015 and 2016, respectively. In 2015, a higher percentage of juvenile salmon was detected between sunrise and solar noon (75.6%), but a similar behaviour was not observed in 2016 (51.9%). A logarithmic relationship between juvenile salmon length and $\Delta MVBS_{67-125}$, the difference between the mean backscattering volume at 67 and 125 kHz, was derived from empirical acoustic and fish net data. The results presented here show that inverted echosounders provide a cost-effective, non-intrusive option for long-term monitoring of fish populations in the area. Further research is required in order to improve our understanding of the acoustic signature of each species, and to develop analysis and automation methods to increase accuracy, efficiency and replicability of the results.

Résumé

L'objectif de cette étude était d'évaluer l'utilisation d'échosondeurs inversés pour la surveillance continue des populations de saumon juvénile dans les Iles Discovery et le Détroit de Géorgie. Quatre échosondeurs à faisceau unique furent déployés en 2015 et cinq furent déployés en 2016, afin de collecter des données sur l'abondance, le comportement et la période de migration du saumon juvenile de mai à septembre. Ce rapport décrit la méthodologie et les résultats primaires obtenus suivant l'analyse des données acoustiques multi-fréquence collectées à un site qui fut répliqué en 2015 et 2016. Ce site est situé dans le chenal d'Okisollo dans les Iles Discovery. La période de migration du saumon juvénile observée au moyen des échosondeurs inversés est en accord avec celle obtenue par l'échantillonnage à la seine mené par MPO. La période de migration a été observée de la mi-mai à la mi-juillet en 2015 et de la mi-mai à la mi-juin en 2016. L'abondance totale était similaire en 2015 et en 2016. La profondeur moyenne des bancs de saumon juvénile était de 5.3 $\pm$ 1.7 m et 3.5 $\pm$ 1 m en 2015 et en 2016, respectivement. L'étendue verticale moyenne des bancs était de 5.9 $\pm$ 0.9 m et 4.9 $\pm$ 1 m en 2015 et 2016, respectivement. En 2015, un plus grand pourcentage des saumons juvéniles ont été observés entre le levé du soleil et le midi solaire (75.6%). Toutefois, une tendance similaire n'a pas été observée en 2016 (51.9%). Une relation logarithmique est établie entre la longueur moyenne des saumons juvéniles et $\Delta\mathrm{MVBS}_{67-125}$, la différence entre la rétrodiffusion volumique moyenne à 67 et 125 kHz, à partir des données empiriques. Les résultats présentés dans ce rapport montrent que l'utilisation d'échosondeurs inversés peuvent fournir un moyen rentable et non invasif d'effectuer la surveillance à long terme des stocks de saumon juvénile, lorsque la connaissance préalable de l'écologie du milieu est suffisante. Des recherches additionelles sont nécessaires afin d'améliorer notre compréhension de la signature acoustique de chaque espèce détectée et de développer des méthodes d'analyse et d'automatisation qui augmenteront la précision, l'efficacité et la reproductibilité des résultats.

1 Introduction

Long-term monitoring of marine fish populations has long been conducted using standard fish sampling methods, such as trawling and purse seining. From the early 1980s to 1990s, significant improvements in hydroacoustic methods and technologies have allowed for the use of vessel-mounted echosounders to conduct large spatial surveys of fish stocks (Dickie et al., 1983, 1987; Foote et al., 1987; Johannesson and Mitson, 1983; MacLennan et al., 1990; Rose et al., 1988; Simmonds et al., 1991). Combined, trawl and acoustic methods are highly efficient to map distributions and abundances over large areas. However, they are generally restricted to a few surveys per year, and are therefore not practical when looking at temporal variability in abundances and distributions. In addition, to allow inter-annual comparability, these surveys are highly restricted in time and might miss important time-sensitive events, leading to a misunderstanding of the ecology and species interactions in the area.

Fixed echosounders have been used extensively in the study of near-surface bubbles and wave processes (Thorpe 1986, Vagle et al., 1992, Trevorrow, 2003). More recently, they have been used to study zooplankton and pelagic fish distribution and behaviour (Thomson et al., 2000; Kaartvedt et al., 2009, Sato et al., 2013). The recent development of several ocean observatories (Favali et al., 2015) have sparked an increase in the number of moored inverted echosounders deployed for long-term monitoring of pelagic communities (Pawlowvicz and McLure, 2010).

In this study, we evaluate the use of inverted, bottom mounted echosounders to monitor juvenile salmon migration timing and distribution in the Discovery Islands and Johnstone Strait, which constitutes a key area in terms of understanding juvenile salmon mortality during their passage from lower British Columbia rivers to the Pacific ocean. We further suggest that moored inverted echosounders can provide insightful data on the behaviour, abundance and migration timing of juvenile salmon and prove to be a non-invasive, cost-effective approach for long-term monitoring purposes.

2 Materials and Methods

2.1 Study area and survey design

Located between the eastern side of central Vancouver Island and the British Columbia mainland, the Discovery Islands area is made of a complex network of narrow channels and deep fjords (Foreman et al., 2012). Water circulation is dominated by tides, with strong currents occurring in Johnstone Strait, while lowest tidal currents are observed southeast of Quadra Island and in Kanish and Waiatt Bay in the north (Figure 1, Foreman et al. 2012).

Moored inverted echosounders were deployed at several locations in the Discovery Islands and Johnstone Strait area in 2015 and 2016 to collect data primarily during the expected juvenile salmon migration period, which usually extends from early May to July. Four moorings were deployed in 2015 and five moorings were deployed in 2016 (Figure 2). Tables 1 and 2 give a summary of the data collected at each site.

In 2015 and 2016, two of the four moorings were deployed in Okisollo channel, a sheltered body of water separating the islands of Sonora and Quadra. This area is known as a juvenile salmon hotspot in May and June, and is also home to several Atlantic salmon aquaculture sites (Figure 3). In 2015, two additional sites were deployed in Johnstone Strait, one near Chatam Point and one near Sayward. The latter is located near DFO's primary purse seining site for monitoring juvenile salmon. These sites presented some analytical challenges due to the presence of bubbles caused by surface waves which contaminated the acoustic signal. Signal from these bubbles is stronger than that of fish schools, greatly reducing the usefulness of the acoustic data during periods of strong winds. In 2016, the three moorings not deployed in Okisollo channel were deployed at Channe Island, Hoskyn channel and Knox Bay. These sites cover several possible pathways for juvenile salmon migration through the Discovery Islands and are accessible by the purse seiner. These locations were chosen in order to reduce chances of bubble contamination.

2.2 Data collection

2.2.1 Echosounders and RBRs

Each mooring consisted of a bottom-mounted AZFP echosounder (Acoustic Zooplankton and Fish Profiler, ASL Environmental Sciences), one or two

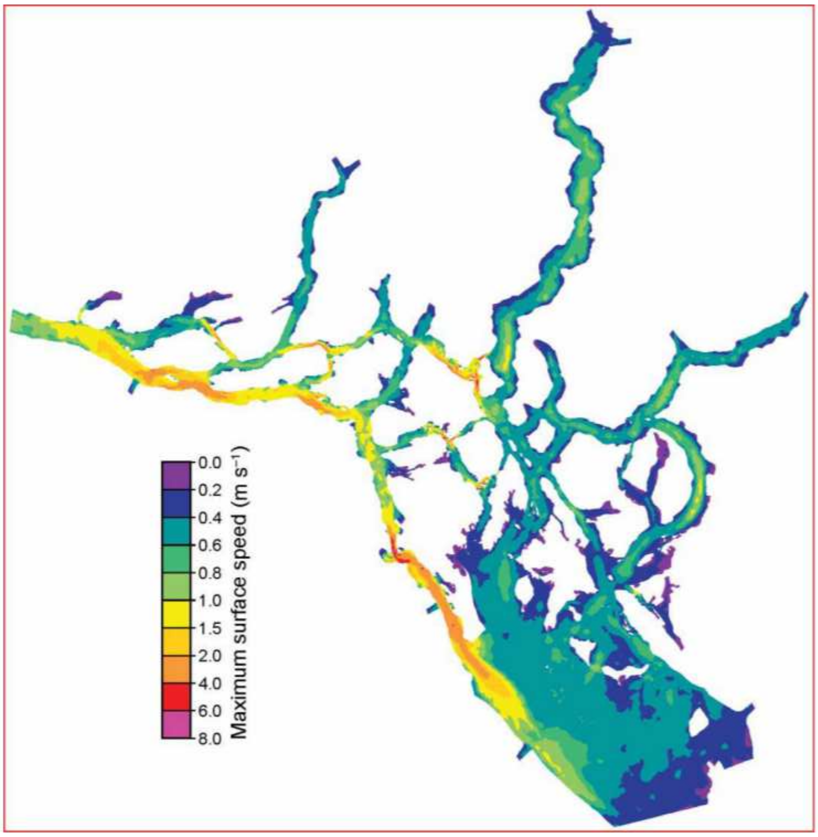

Figure 1: Maximum surface speeds (ms^{-1}) over a 28-day model simulation period (April 1- 28 2010) (Foreman et al., 2012).

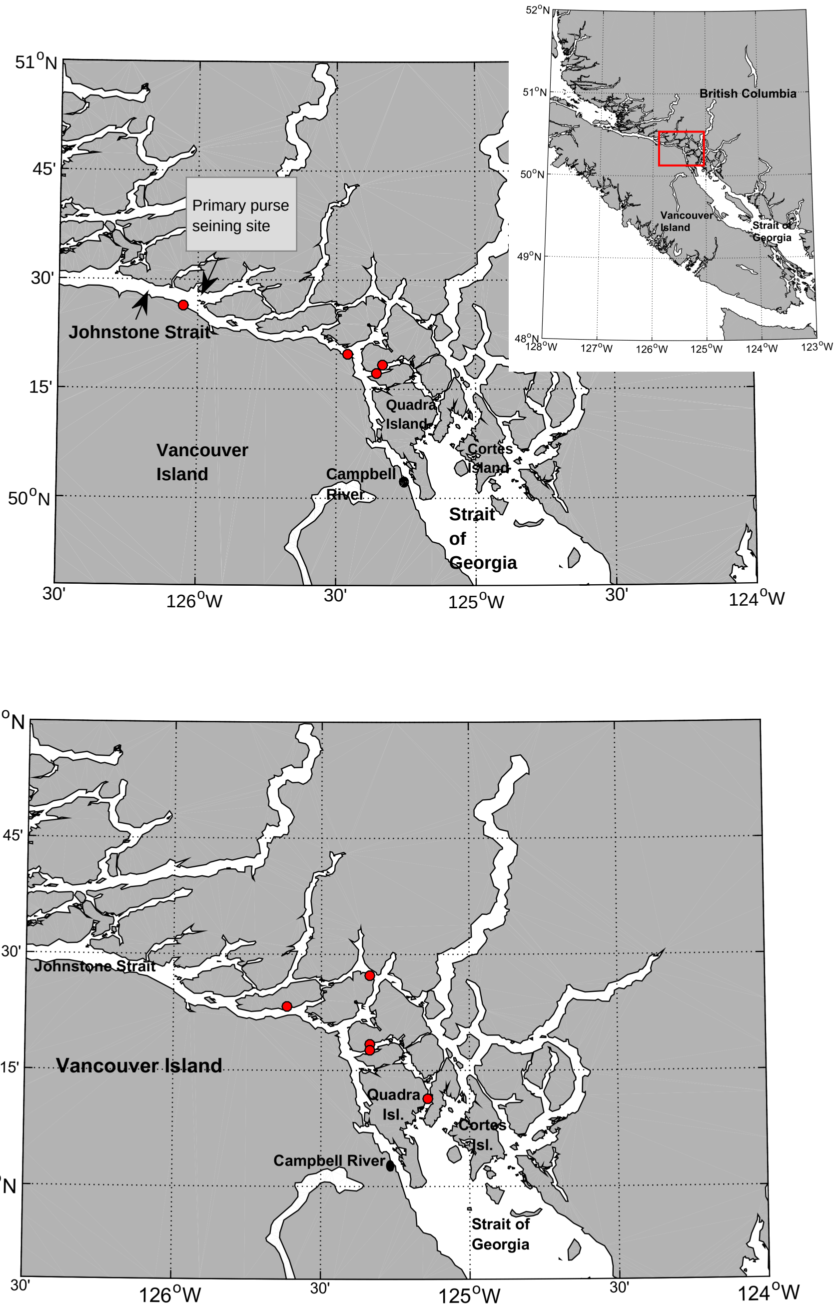

Figure 2: Upper panel: Location of the four moorings (red dots) deployed in the Discovery islands and Johnstone strait area from May to October 2015. Lower panel: Location of the five moorings (red dots) deployed in the Discovery islands area from May to October 2016.

Figure 3: Upper panel: Location of AZFP moorings in Okisollo channel in 2015 and 2016. The "secondary" mooring was only deployed in 2016, whereas the "deep" mooring was deployed in 2016. The primary mooring was deployed both years. Middle panel: Location of primary mooring site in Okisollo channel in relation to Cermaq aquaculture farm. Lower panel: Location of secondary mooring deployed in Okisollo channel in 2015 near Brent Island.

Site	Location	Coordinates	AZFP serial #	Frequency (kHz)	Bottom depth (m)	Start date/time	End/date time
1	Venture Pt.	$\frac{50.3057^{\circ}N}{125.3348^{\circ}W}$	55084	$\frac{67/125}{200/455}$	55	2015-05-13 14:28	2015-09-30 11:20
2	Brent Isl.	$\frac{50.2861^{\circ}N}{125.3538^{\circ}W}$	55086	$\frac{67/125}{200/455}$	53	2015-05-14 9:41	2015-09-30 11:20
3	Chatam Pt.	$\frac{50.3308^{\circ}N}{125.4603^{\circ}W}$	55026	200	43	2015-05-14 12:50	2015-09-30 7:59
4	Johnstone St.	$\frac{50.4392^{\circ}N}{126.0537^{\circ}W}$	55085	$\frac{67/125}{200/455}$	33	2015-05-15 6:00	2015-09-30 11:20

Table 1: Summary of 2015 data collection.

Site	Location	Coordinates	AZFP serial #	Frequency (kHz)	Bottom depth (m)	Start date/time	End/date time
1	Venture Point	$\frac{50.3060^{\circ}N}{125.3343^{\circ}W}$	55086	$\frac{67/125}{200/455}$	61	2016-05-11 15:05	2016-09-15 22:56
2	Okisollo mid-channel	$\frac{50.2939^{\circ}N}{125.3377^{\circ}W}$	55124	67	110	2016-05-11 11:27	2016-09-28 14:59
3	Knox Bay	$\frac{50.3871^{\circ}N}{125.6161^{\circ}W}$	55085	$\frac{67/125}{200/455}$	52	2015-05-12 10:36	2015-09-17 23:59
4	Channe Island	$\frac{50.4538^{\circ}N}{125.3363^{\circ}W}$	55026	200	58	2015-05-10 15:00	2015-10-01 23:59
5	Hoskyn channel	$\frac{50.1901^{\circ}N}{125.1419^{\circ}W}$	55084	$\frac{67/125}{200/455}$	54	2015-05-13 11:50	2015-09-22 02:19

Table 2: Summary of 2016 data collection.

temperature and pressure sensors (RBR Ltd.), and an acoustic release (figure 4). Three of the AZFP echosounders operated at four frequencies (67, 125, 200, and 455 kHz); the remaining two operated at one frequency (67 and 200 kHz). In the multi-frequency units, the elements for the three higher frequencies are located within a single transducer unit; the larger 67 kHz transducer requires a single housing unit. The two transducers were located approximately 30 cm from each other over a metal frame (figure 5). Each echosounder was calibrated by the manufacturer prior to deployment and after recovery.

The AZFP hardware can be set to operate under different parameter settings and/or ping regime during a single deployment. Each setting is called a phase. Tables 3 to 6 describe the settings used for each station and phase.

	Site 1		Site 2		Site 3	Site 4	
Phase	1	2	1	2	1	1	2
Burst interval (s)	3	5	3	5	1	2	5
Pings per burst	1	1	1	1	1	1	1
Ping period (s)	3	5	3	5	1	2	5

Table 3: AZFP settings for each site and phase in 2015. Phase 1: Start of recording to August 01. Phase 2: August 01 to end of recording.

	Site 1		Site 2		Site 3		Site 4		Site 5	
Phase	1	2	1	2	1	2	1	2	1	2
Burst interval (s)	3	5	2	4	3	5	1	2	3	5
Pings per burst	1	1	1	1	1	1	1	1	1	1
Ping period (s)	3	5	2	4	3	5	1	2	3	5

Table 4: AZFP settings for each site and phase in 2016. Phase 1: Start of recording to August 01. Phase 2: August 01 to end of recording.

	Site 1		Site 2		Site 3	Site 4	
Frequency (kHz)	67	125/200/455	67	125/200/455	200	67	125/200/455
Pulse duration (μs)	500	300	500	300	300	500	300
Digital rate (kHz)	64	64	64	64	64	64	64

Table 5: AZFP settings for each site and frequency for the 2015 sampling season.

	Site 1		Site 2	Site 3		Site 4	Site 5	
Frequency (kHz)	67	125/200/455	67	67	125/200/455	200	67	125/200/455
Pulse duration (μs)	500	300	500	500	300	300	500	300
Digital rate (kHz)	64	64	64	64	64	64	64	64

Table 6: AZFP settings for each site and frequency for the 2016 sampling season.

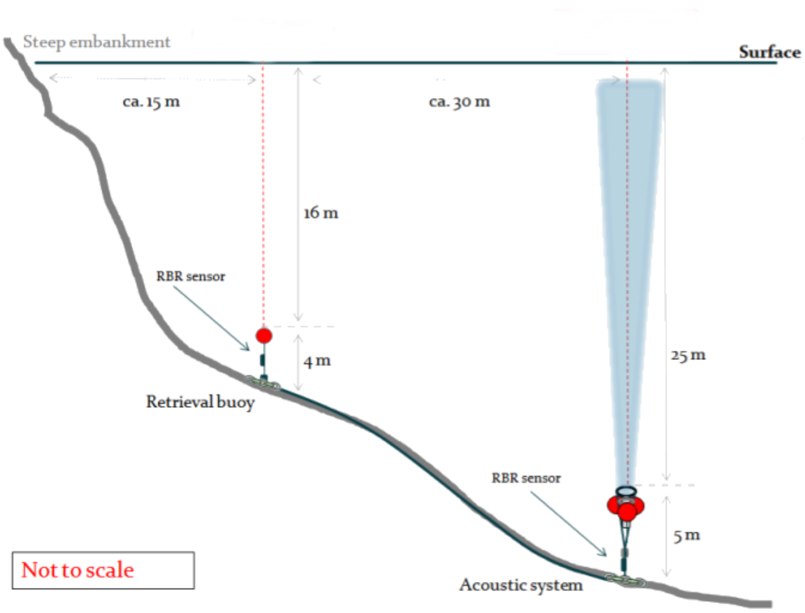

Figure 4: Mooring schematic

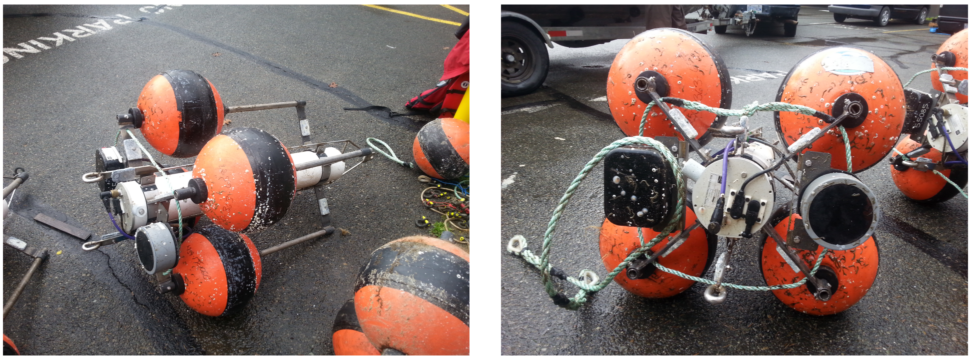

Figure 5: Multi-frequency AZFP echosounders (ASL Environmental Sciences) after being recovered from Okisollo channel in 2016.

Sampling rate was selected in order to maximize data resolution during expected high juvenile salmon presence (May to July) but was limited by battery consumption and memory usage.

In order to resolve single acoustic targets from the received echo, the range difference between target 1 and target 2 must be large enough for the two echoes not to overlap (Simmonds and MacLennan, 2005):

$$R_2 - R_1 = \frac{c\tau}{2} \quad (1)$$

where c is the speed of sound in seawater ($\sim$ 1500 ms^{-1}) and τ is the pulse duration (s). Given a pulse duration of 500μs at 67 kHz and 300μs at 125, 200 and 455 kHz, the minimum single target resolution distance is 37.5 cm and 22.5 cm, respectively.

2.2.2 CTD casts

CTD casts were collected throughout the summers of 2015 and 2016 in the area of study by various DFO sampling programs. These casts were used to determine the monthly average profile of sound speed and absorption coefficient at each station to be used in the post-processing stages of data analysis (see appendix 1).

2.2.3 Purse seine

Purse seine surveys were conducted twice a week by Fisheries and Oceans Canada from May 12 to July 15 in 2015 and from May 17 to July 13 in 2016. Sampling was performed with a small mesh purse seine on a commercial seiner during slack and low flow tides to ensure that the net opening remained stable during fishing operations and that catch-per-unit-effort (CPUE) was comparable among sampling events. A summary of fish species, abundances as well as lengths of juvenile salmon can be found in appendix 2.

2.2.4 DIDSON

Short acoustic surveys using a vessel-mounted, side-looking sonar (DIDSON) were conducted above and around all mooring sites in June and July of 2015 and 2016. The DIDSON is a low-range, high resolution sonar, which allows detection of near surface targets such as juvenile salmon. Alongshore transects at increasing distance from the shoreline were conducted to provide information on the fine-scale spatial dynamics in the area of the moorings. This data was also compared to the bottom-mounted acoustic data to improve certainty in target identification. The DIDSON software (v5.26.06) was used for fish counting.

2.3 Data analysis

2.3.1 Computation of Sv and TS

All acoustic analyses were performed with Myriax Echoview (version 7.1), R (version 3.3.1) and Matlab (version 8.5). The mean volume backscattering strength (S_v) and the target strength (TS) are calculated as follows:

$$TS = EL_{max} - \frac{2.5}{a} + \frac{N}{26214a} - TVR - 20logV_{TX} + 40logR + 2\alpha R \quad (2)$$

$$S_v = EL_{max} - \frac{2.5}{a} + \frac{N}{26214a} - TVR - 20logV_{TX} + 20logR + 2\alpha R - 10log(\frac{c\tau\psi}{2}) \quad (3)$$

where EL_{max} is the echo level (in dB re 1 μPa) at the transducer that produces full-scale output; N, in counts, is linearly related to the input voltage after it has been amplified, bandpass filtered, and passed through a so-called "detector" whose output is a function of $\log(v_{in}^2)$; a is the slope of the detector response; TVR is the transmit voltage response of the transducer in dB re 1 μPa/volt at 1 m range; V_{TX} is the voltage amplification factor before it is sent out; α is the absorption coefficient; c is the sound speed; and τ is the pulse length. R is the range calculated as $R = ct/2$. $40logR + 2\alpha R$

and $20logR + 2\alpha R$, in equations 2 and 3, respectively, represent the time-varied-gain (TVG) applied to compensate for transmission loss (TL). ψ, the equivalent-beam-angle, is approximated by

$$\psi = 1.4\pi(1 - cos\theta) \tag{4}$$

where θ is half the full -3 dB beam angle of the transducer. For more information on the conversion from voltage to acoustic signal specific to the AZFP, please refer to ASL Environmental's AZFP Operator's Manual.

The echograms were treated in their original, reversed perspective with the tidal amplitude evident at the top (figure 6). This method allowed for easier correction of range-dependent noise issues such as side-lobe and TVG. The depth was estimated as an offset from the detected surface.

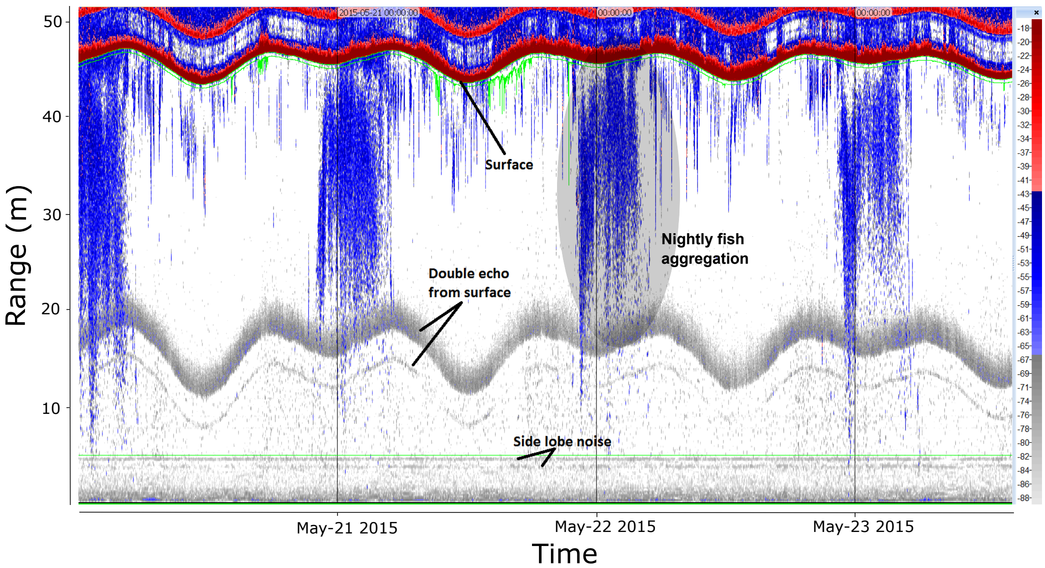

Figure 6: Example of a typical echogram showing surface backscatter (with tidal pattern visible) and large nightly aggregations (shaded). Noise from surface double echo and side lobes are also indicated.

2.3.2 Defining the surface and removing bubble noise

Echoview's *best bottom candidate* algorithm was used to detect and define backscatter from the surface. The resulting line was smoothed to exclude higher frequency variations caused by waves and other strong signals such as fish schools, using a 49 pings (maximum window permitted by the Echoview operator) running window filter selecting the maximum detected range (shallowest depth) within that interval. The resulting line was reviewed manually and used as the surface reference.

Bubbles originating from surface waves were sometimes found to contaminate the acoustic data near the surface. In particular, deep bubble entrainment generated acoustic noise down to depths of 20 m at our two Johnstone Strait sites in 2015. In 2016, care was taken to ensure that moorings were deployed in regions of minimal wind-generated waves. However, it was not possible to completely avoid bubble noise near the surface. To exclude this signal from the analysis, an exclusion line was generated from the 125 kHz data using Echoview's *Maximum Sv* algorithm. Data at 125 kHz were used because the acoustic signal from bubbles is often stronger at this frequency (Trevorrow et al., 1993). The exclusion line was reviewed and corrected manually when fish schools at the surface were mistakenly selected as surface waves. To help separate bubbles from fish signals during the manual correction, the difference between the 67 and 125 kHz frequencies (ΔMVBS) was used. Whereas the acoustic signal from fish is fairly stable across frequencies, bubbles backscattering properties are frequency-dependent.

An offset of 0.3 m was applied to the final line delineating the lower limit of bubble noise. Data above this line, as well as data below a 5 m distance from the transducers' face, where side lobes had more effects, were excluded from the analysis.

2.3.3 Background noise removal

Background noise was removed by linear subtraction using Echoview's *Background Noise Removal* algorithm (DeRobertis and Higginbottom, 2007). Thresholds for maximum estimated noise were -125 dB at 67, 125 and 200 kHz, and -110 dB at 455 kHz and were determined empirically. A signal-to-noise ratio of 10 dB specified the acceptable limit for a signal to be deemed distinguishable from noise.

2.3.4 School detection and classification

Fish schools were detected using Echoview's school detection module (Barange, 1994, Coetzee, 2000). Table 7 shows the selection parameters for school detection. The 67 kHz echogram was smoothed (20 samples x 9 pings mean in the linear domain) and a -67 dB threshold applied prior to running the module. This threshold was chosen in order to include as much of the signal

Parameters	Value
Minimum threshold (dB re m^{-1})	67
Minimum total school length (s)	24
Minimum total school height (m)	1
Minimum candidate length (s)	20
Minimum candidate height (m)	1
Maximum vertical linking distance (m)	2
Maximum horizontal linking distance (s)	20

Table 7: Parameters used for the school detection module in Echoview.

from fish as possible, while excluding noise from the second surface echo. The resulting smoothed and thresholded echogram was only used to define the perimeter of the fish schools, not to export the acoustic variables.

Echoview's region classification module was used to separate the detected schools into categories, which were further inspected visually. Here, we focus on two school categories: the near-surface schools were ascribed to juvenile salmon based on the purse seine, visual surveys, and the DIDSON data collection. In 2015, juvenile salmon prevailed by 90% over herring in 31 out of 36 purse seine samples collected. This number increased to 100% in 2016. Deeper, elongated schools with higher acoustic densities were consistent with herring. However, since we lack validation data for this category, we classify them as "high density" schools (figure 7).

Table 8 shows the selection parameters used for the classification of the two class categories. Note that Echoview requires GPS input in order to run the school detection algorithm. In this case, we converted the units of the horizontal axis by creating an imaginary GPS linear track of 1 knot (0.51 m/s).

Class	Parameters	Value
Juvenile salmon	Samples in domain	230 - 50 000
	Thickness mean (m)	1.6 - 18
	Uncorrected length (m)	15 - 930
	Range mean (m)	>25
	Sv mean (dB)	<-48
High density	Samples in domain	NC
	Thickness mean (m)	5 - 20
	Uncorrected length (m)	<600
	Range mean (m)	NC
	Sv mean (dB)	>-48

Table 8: Parameters used for the region classification algorithm in Echoview. "NC" means that no constraints were applied for this parameter.

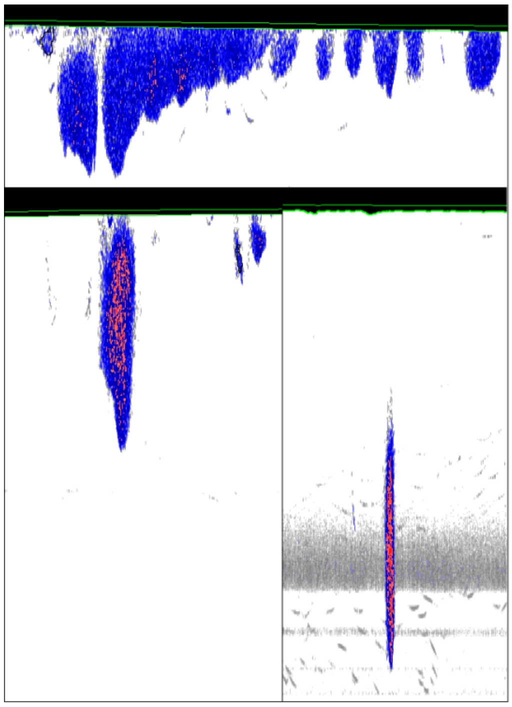

Figure 7: Example of a typical acoustic signal for juvenile salmon schools (upper panel) and for suspected herring (hereafter named high density schools, lower panel).

2.3.5 Computation of NASC and fish density

NASC, or nautical area scattering coefficient (m^2/nmi^2) is a measure of acoustic signal per surface area:

$$NASC = 4\pi \times 1852^2 \times 10^{\frac{S_v}{10}} \times T \tag{5}$$

where T is the thickness (vertical extent) of the analysis domain and S_v the mean volume backscattering strength. Here, we use the entire water column contained in the analysis domain as T. The Elementary Time Sampling Unit, or ETSU, is defined as the length of time on which the acoustic measurements are averaged to give one sample. In this study, we use 1 day as ETSU unit to explore seasonal variations in NASC, and we use 1 hour as ETSU unit to explore relationships between NASC and daily cycles such as tides and light.

The density of fish per unit area (ρ_a) is defined as:

$$\rho_a = \frac{NASC}{4\pi \times \sigma_{bs}} \tag{6}$$

where

$$\sigma_{bs} = 10^{\frac{TS}{10}} \tag{7}$$

Thus, assuming homogeneous schools of identical species and similar size, and a random distribution of fish within the beam (Parker-Stetter et al., 2009), fish density is linearly proportional to NASC. NASC is calculated for fish schools only from the non-averaged, non-thresholded data.

2.3.6 Difference in mean backscattering volume

The difference in mean backscattering volume (ΔMVBS) between one or more frequency pairs is commonly used to separate acoustic scatterers into categories. The efficacy of this method varies; it has been used successfully to distinguish zooplankton from other scatterers like fish because the echoes from plankton are more highly dependent on frequency than the echoes from fish (Lavery et al., 2007). A number of studies also discuss the potential of using this method to differentiate between species of fish (DeRobertis et al., 2010; Sato et al., 2015). Here, we use this method as a post-classification validation method for the choice of our two main classes (Juvenile salmon and High density), and to develop a relationship between mean fish length and ΔMVBS.

Acoustic backscatter differences for all possible frequency pairs (67, 125 and 200 kHz) were calculated for each averaged cell (30 seconds x 0.5 m mean in linear domain) of the S_v analysis domain. The 455 kHz frequency was excluded from this analysis because the signal-to-noise ratio increased too rapidly with range at this frequency to allow for an accurate comparison with the other frequencies.

A difference in backscatter in the logarithmic domain is equivalent to its ratio in the linear domain:

$$S_{vf_2} - S_{vf_1} = s_{vf_2}/s_{vf_1} \tag{8}$$

where $S_v = 10log_{10}s_v$, and s_v is the volume backscattering coefficient (MacLennan et al., 2002).

To minimize the effects of background noise in each cell, only cells where the mean backscattering volume (MVBS) was greater than -70 dB for at least one of the frequencies in the pair were used for further analysis.

3 Results and discussion

Results presented here focus on the data collected at the site located near Venture Point, in Okisollo channel during the 2015 and 2016 spring and summer seasons.

3.1 Spatial series

The spatial surveys conducted with the DIDSON offer a fine-scale overview of the local dynamics of juvenile salmon in the area of the mooring (figure 8). The area was surveyed a total of 13.2 hours over 7 days in 2015, and 16.2 hours over a period of 5 days in 2016. All surveys were conducted in June and July.

The spatial surveys reveal patchiness in the juvenile salmon distribution. In both years, a higher abundance was found at a small bay located north of the echosounder location. Overall, a higher abundance and a wider distribution throughout the survey area was detected in 2016.

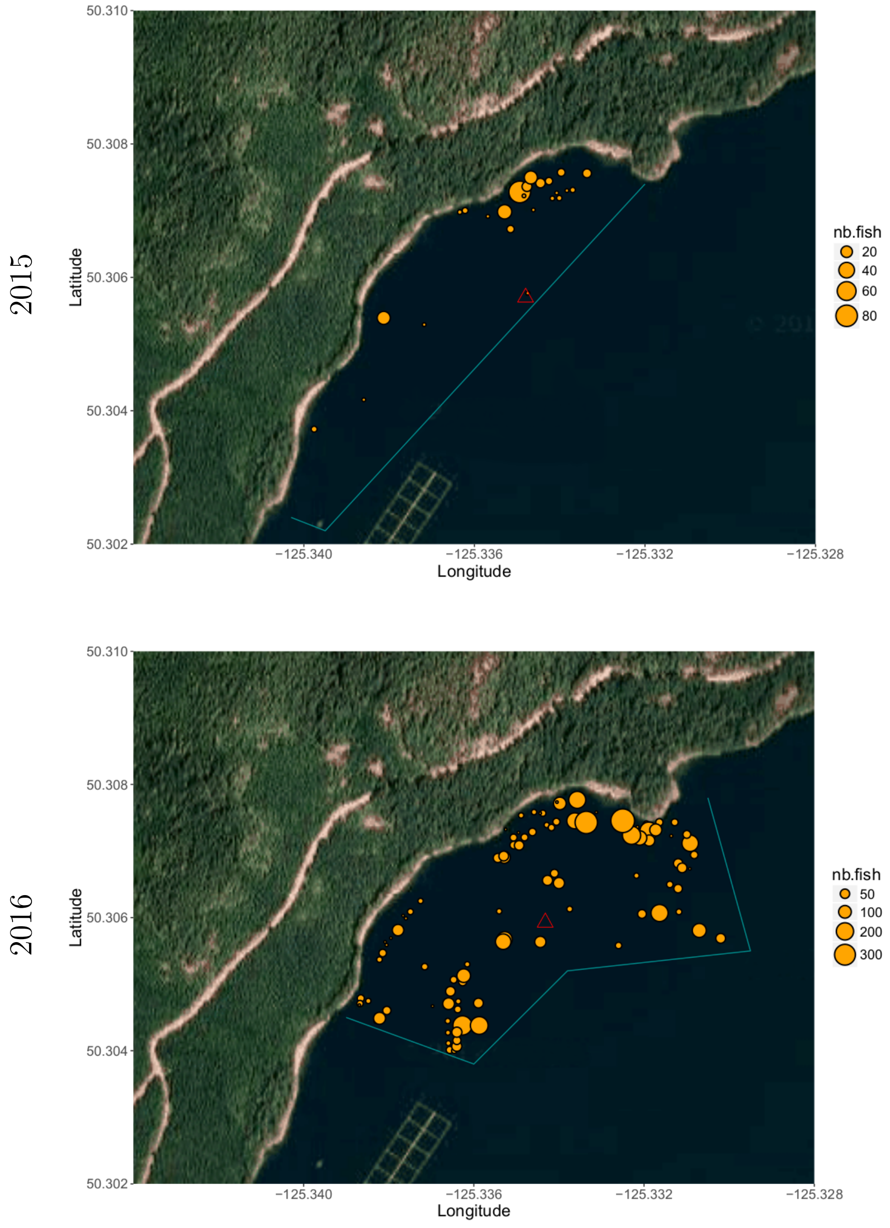

Figure 8: Spatial distribution of juvenile salmon in the vicinity of site 1 as obtained from the DIDSON surveys in 2015 and 2016.

3.2 Migration timing

In both 2015 and 2016, sockeye was the main species of juvenile salmon collected by the purse seiner (appendix 1). A lower abundance of chum was also present, while pink was found in numbers similar to chum in 2016.

Both years show a very good agreement between the migration timing observed by the purse seiner and the acoustic data (Figure 9). In 2015, the peak migration was observed between mid-May and mid-July. The high resolution acoustic data shows an early peak in abundance (May 22) that is not reflected in the purse seine data. The second peak detected on June 6 matches the main peak observed with the purse seiner on June 9. After July 15, very little acoustic signal from juvenile salmon was detected, coinciding with the end of the purse seine sampling season.

In 2016, NASC from juvenile salmon was consistently high from mid-May to mid-June, where it quickly decreased to low values, in contrast with the more widespread and variable NASC values observed in 2015. The total cumulative NASC was similar in 2015 and in 2016, whereas the total juvenile salmon catch by the purse seiner was almost 4 times higher in 2016. NASC time series also suggest that in both years, as the biomass of juvenile salmon decreased, it was replaced by an increased biomass of the high density schools, which are presumably composed of herring (Figure 9, lower panel).

3.3 Behaviour

In 2015, during peak juvenile salmon abundance (mid-May to mid-July), mean schools depth was 5.3 ± 1.7 m (figure 10). In 2016, it was shallower (3.5 ± 1 m from mid-May to mid-June). The mean vertical extent of the juvenile salmon schools was 5.8 ± 0.9 m in 2015 and 4.9 ± 1 m in 2016. The beam occupancy, which is the vertical extent of the schools multiplied by the time it spent within the acoustic beam, suggests that during both sampling seasons, the juvenile salmon schools were larger and more continuous above the beam at the very beginning of the peak abundance, in May.

The mean depth of high density schools was 18.4 ± 8.7 m and 30.7 ± 7.9 m, and their vertical extent was 14.4 ± 5.9 m and 13.3 ± 5.6 m (2015 and 2016, respectively).

In 2015, there was a net preference for juvenile salmon presence between sunrise and solar noon (75.6% of NASC). However, this behaviour was not

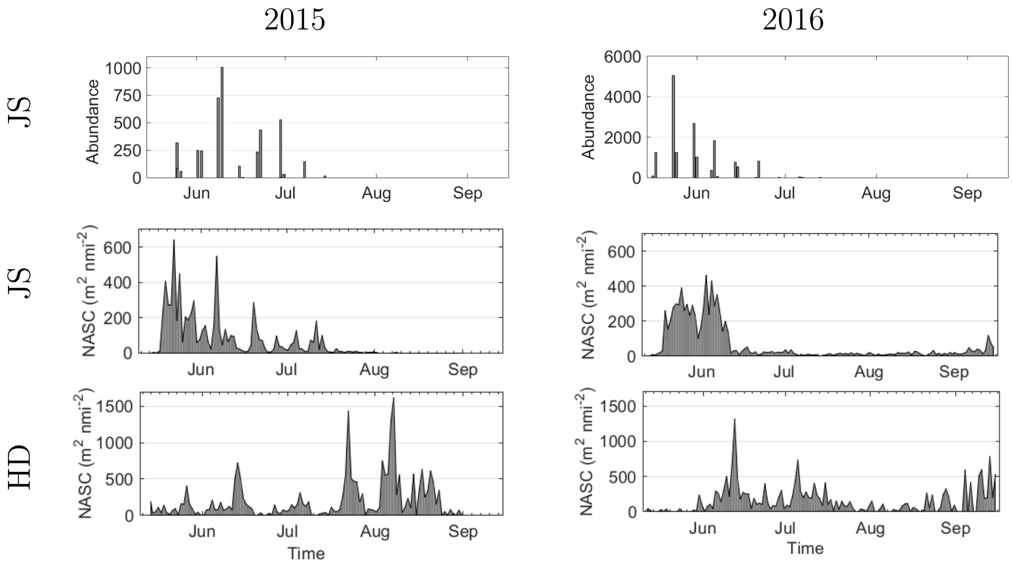

Figure 9: Upper panel: Number of juvenile salmon (all species) caught in Okisollo channel by the purse seiner in 2015 and 2016. Middle and lower panels: Daily NASC of juvenile salmon (JS) and high density (HD) schools at site 1 in 2015 and 2016.

observed in 2016, where only 51.9% of the NASC was observed between sunrise and solar noon (figure 11), the remaining occurring between solar noon and sunset.

Using hourly ETSU, we estimated the percentage of NASC from juvenile salmon that occurred at each time of day and explored a possible relationship with the tidal cycle. No currents data were available in the area; consequently we used pressure data from the RBR sensors mounted on the AZFP frame to estimate a relative velocity using the first derivative of pressure over time. The resulting values of velocity, however, should be taken with caution. The variation in tidal amplitude above the mooring is not necessarily an indication of the currents above it. Deploying ADCPs (Acoustic Doppler Current Profilers) next to the AZFP moorings to record currents in their immediate vicinity would give us a much more accurate picture of the behaviour of juvenile salmon in relation to tidal currents. Nevertheless, the results presented here show some interesting trends that are worth mentioning.

In 2015, although only 60.6% of the abundance of juvenile salmon was detected during decreasing water levels (figure 12), nine out of the ten most

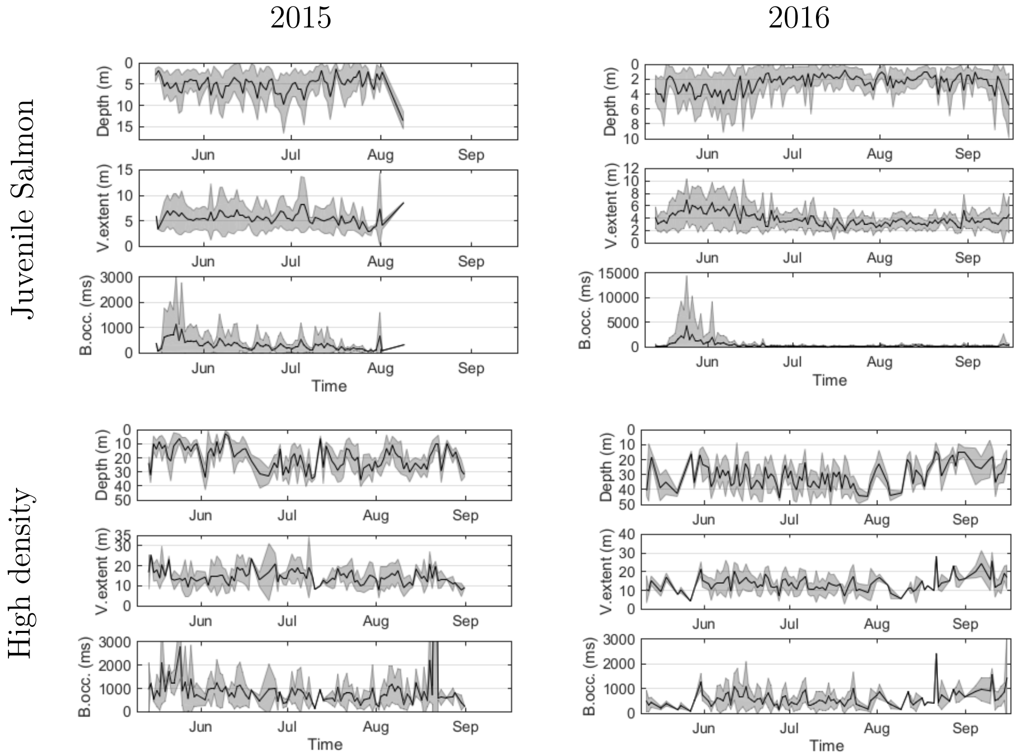

Figure 10: Schools characteristics for juvenile salmon and high density schools at site 1 in 2015 and 2016. In each subplot, upper panel: mean depth of the detected schools; middle panel: vertical extent of the detected schools; lower panel: beam occupancy (in meters per seconds) of the detected schools.

significant juvenile salmon schools were detected during that period, corresponding to 90.7% of the total NASC of these schools. In 2016, only 48.6% of juvenile salmon abundance was detected during decreasing water levels. Keeping only the ten hours of strongest NASC, this percentage decreases to 39.6%.

3.4 ΔMVBS to standard length relationship

We observed a gradual increase in the $\Delta\text{MVBS}_{67-125}$ of juvenile salmon throughout the sampling season (figure 13). This increase is also observed in the standard length of juvenile salmon collected by the purse seiner (figure 14).

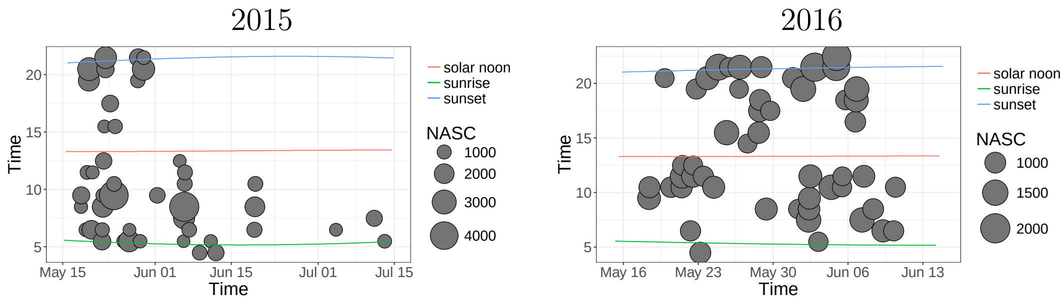

Figure 11: NASC (m^2 nmi^{-2}) as a function of time of day for every hour of the sampling season. A threshold of 800 was applied on minimum NASC value. Three horizontal lines, representing sunrise, solar noon, and sunset, are also represented.

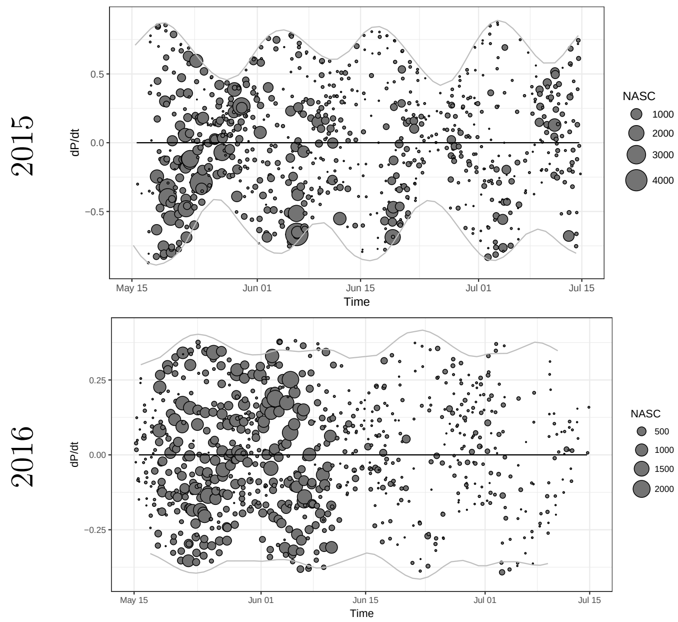

Figure 12: NASC (m^2 nmi^{-2}) as a function of $\frac{dP}{dt}$ at site 1 during spring and summer 2015 (upper panel) and 2016 (lower panel). $\frac{dP}{dt}$ represents the variation in water pressure (equivalent to depth) as a function of time. The most negative values correspond to the fastest decrease in water level, and the most positive values correspond to the fastest increase in water level. Zero corresponds to slack tide. The changing extrema of $\frac{dP}{dt}$, a result of the tidal amplitude varying with the lunar cycle, are represented by gray lines.

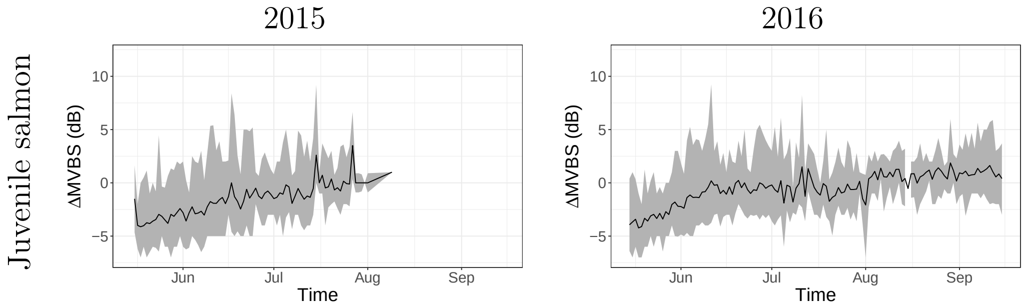

Figure 13: ΔMVBS$_{67-125}$ of juvenile salmon at site 1 (Venture Point, Okisollo channel) during the summer seasons of 2015 and 2016.

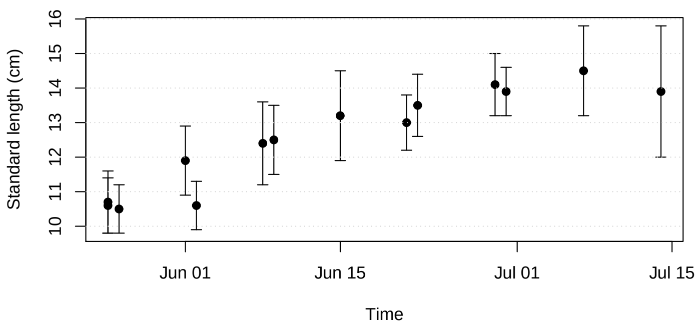

Figure 14: Average length (mm) and standard deviation of juvenile Sockeye and Chum (most common species) sampled by DFO's purse seine program in Okisollo channel in 2015.

Target strength (TS) is related to fish length as follows (Simmonds and MacLennan, 2005):

$$TS = a \log_{10}(L) + b \tag{9}$$

The target strength for an individual fish target is defined as

$$TS = 10 \log_{10}(\sigma_{bs}) \tag{10}$$

where σ_{bs} is the backscattering cross-section (m^2). Combining equations 9 and 10 yields

$$10 \log_{10}(\sigma_{bs}) = a \log_{10}(L) + b \tag{11}$$

σ_{bs} can also be expressed in terms of s_v, the volume backscattering coefficient (m^2 m^{-3}):

$$s_v = \frac{\sum_{n=1}^{N} \sigma_{bs}}{V} \tag{12}$$

where N is the total number of fish and V the sampling volume. Assuming that all fish in the sampling volume have a similar length, equation 12 becomes

$$s_v = \frac{N\sigma_{bs}}{V} \tag{13}$$

This assumption is true only if the observed schools are composed mainly of juvenile salmon individuals of similar-size. Purse seine samples conducted in Okisollo channel in 2015 suggest that this is the case (see figure 14 and appendix B).

S_v, the volume backscattering strength, is defined as the logarithmic transformation of s_v (dB re: 1 m^{-1}):

$$S_v = 10 \log_{10}(s_v) \tag{14}$$

Combining equation 14 with equation 11, we obtain a relationship between $\Delta MVBS_{67-125}$, the difference in mean volume backscattering strength at 67 and 125 kHz, and the mean fish length within the sampling volume:

$$\Delta MVBS = S_{v2} - S_{v1} = c \log_{10}(L) + d \tag{15}$$

Using the empirical data of $\Delta MVBS_{67-125}$ and standard lengths of juvenile salmon collected by the purse seiner in 2015, we obtain a predictive

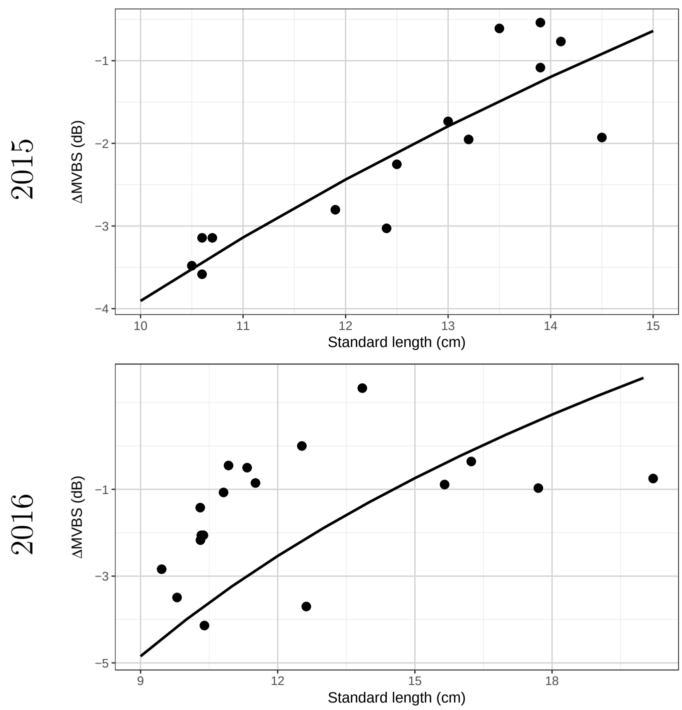

Figure 15: Relationship between standard length (cm) and ΔMVBS (dB) at site 1 in 2015 and 2016. Empirical data is shown as black dots; modeled curve (derived from 2015 data) is shown as solid line. The equation for the logarithmic fit is $\Delta MVBS_{67-125} = 18.5log_{10}(\overline{SL}) - 22.5$.

model for the average standard length of juvenile salmon throughout the sampling season (figure 15):

$$\Delta MVBS_{67-125} = 18.5 log_{10}(\overline{SL}) - 22.5 \tag{16}$$

3.5 Night aggregations

In 2015, large aggregations were detected at night throughout most of the sampling season (figure 16). These aggregations can be separated into two distinct layers: 1) a thin layer aggregating in the upper several meters near the surface; 2) a large layer covering most of the water column above the echosounder accompanied with vertical migration at dawn and dusk. In 2016, this large layer was only detected occasionally, resulting in a greatly reduced NASC in comparison to 2015 (figure 17). On the other hand, the thinner, near-surface layer was detected consistently.

Here we suggest that the thin, near-surface aggregations are composed of juvenile salmon while the larger, deep aggregations are composed of other fish, presumably herring. Age-1 Pacific herring were common in the purse seine samples and are known to exhibit diel vertical migrations (Mackinson, 1999, McCarter et al., 1994). In May 2016, a purse seine sample was collected at night to investigate the nature of the nightly aggregations - the large sample was composed of juvenile Sockeye by 97%, supporting this hypothesis. Unfortunately, no night samples were collected in 2015, thus we can only speculate on the composition of the deeper aggregations.

Figure 17 also shows the depth of maximum volume backscattering strength (Sv), as well as the vertical extent of the nightly aggregations throughout the sampling season in 2015 and 2016. Aggregations were spread from the surface to approximately 25 m depth. During peak 2016 juvenile salmon abundance, from mid-May to the first week of June, the nightly aggregations were mostly found near the surface. After peak abundance, they were larger and spread deeper into the water column.

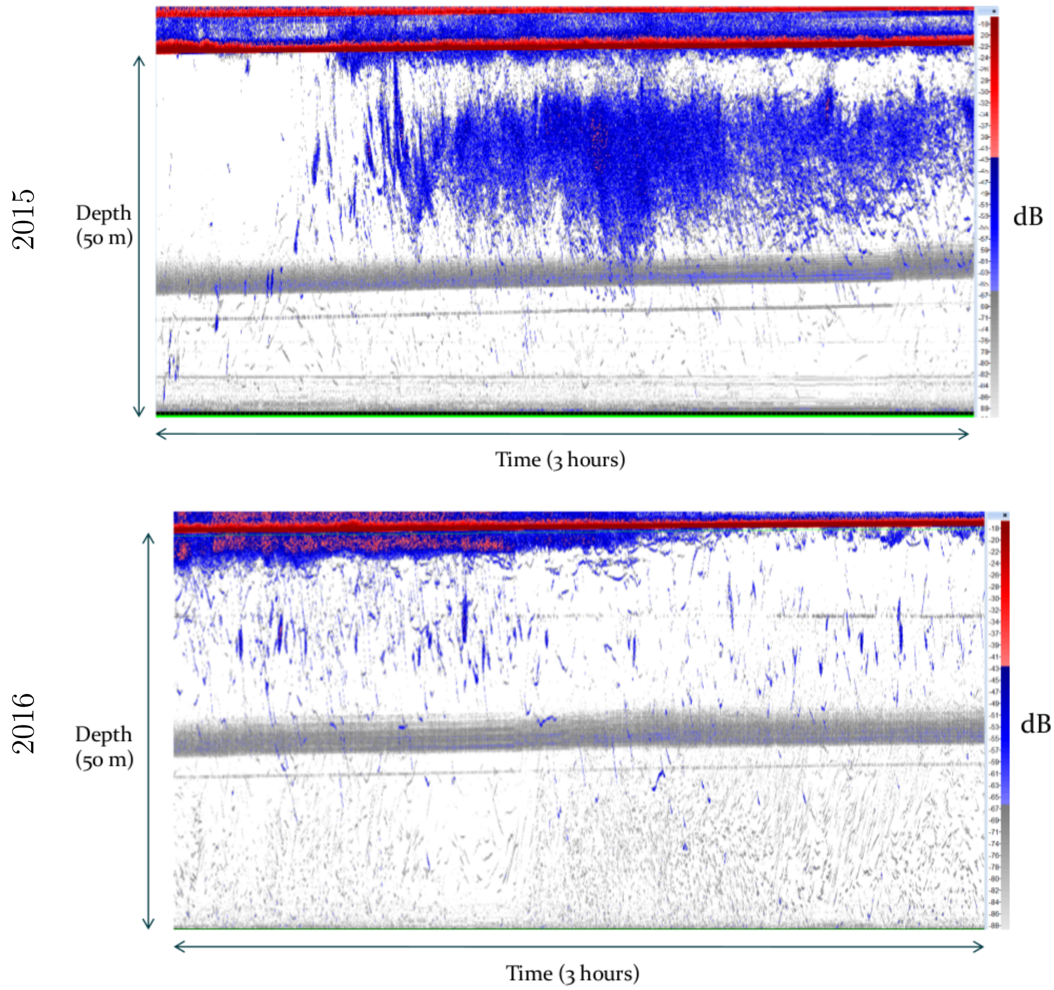

Figure 16: Upper panel: Echogram of a nightly aggregation detected in Okisollo channel on June 1-2 2015 (23h00-02h00). Lower panel: Echogram of a nightly aggregation detected in Okisollo channel on May 22 2016 (00h00-03h00).

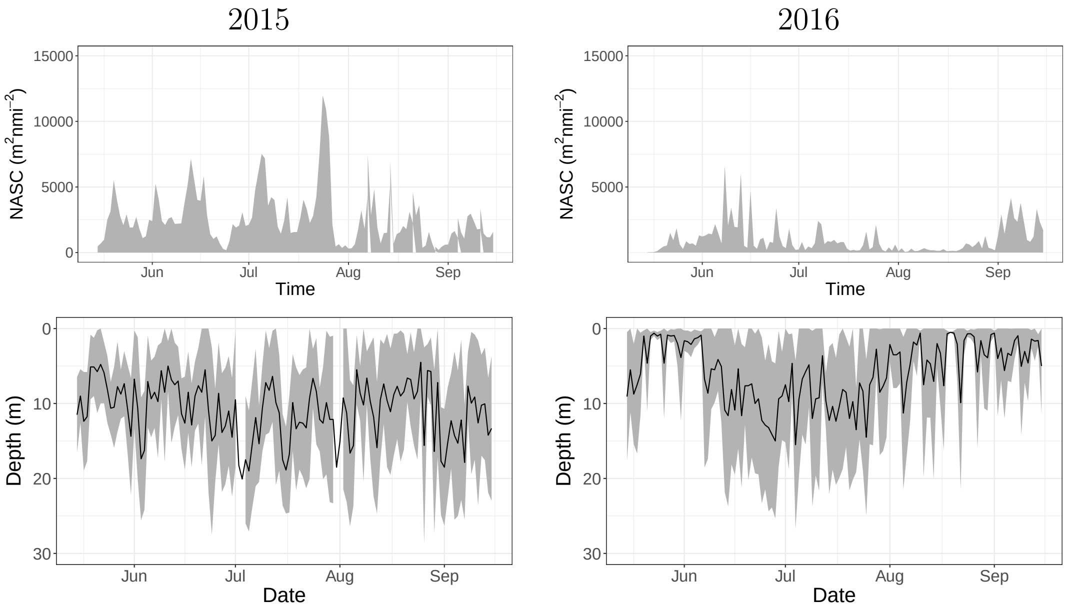

Figure 17: Time-series of the nautical area scattering coefficient (NASC) (upper panel) and the mean depth of maximum volume backscattering strength (Sv) (lower panel) of the aggregations observed at night in 2015 and 2016.

4 Conclusion

This study shows that moored inverted echosounders can provide an efficient, non-invasive and cost-efficient means of monitoring juvenile salmon abundance, distribution and migration in the Discovery Islands. We were able to establish with good accuracy the migration timing of juvenile salmon through Okisollo channel and validated our results with other monitoring programs in the area. The use of an inverted echosounder provided high temporal resolution of juvenile salmon presence in Okisollo channel as well as information on their vertical distribution.

A relationship between the frequency response of juvenile salmon and their average length was established using empirical acoustic and fish length data, suggesting that it is possible to monitor the size of juvenile salmon acoustically. Improvement of the accuracy of this relationship is however required through additional data collection.

We are currently working on developing automation methods for the detection and classification of acoustic targets. In addition, further research is required in order to improve our understanding of the acoustic signature of the species observed in Okisollo channel, through validation of the acoustic data with concurrent fish and zooplankton net data.

5 Acknowledgements

We gratefully acknowledge all those who contributed to this project. George Conkrite, Chelsea Stanley, Svein Vagle and John Morrison provided help with the deployment and recovery of the moorings. Mike Dempsey and Jonathan Poole helped design and assemble the AZFP moorings. Benjamin Snow and Tyler Zubkowski participated in the DIDSON surveys. The Hakai foundation provided CTD data from Hoskyn channel. This project was funded through the Aquaculture Collaborative Research and Development Program (ACRDP) in association with the BC Salmon Farmers Association (BCSFA).

6 References

Barange, M. 1994. Acoustic identification, classification and structure of biological patchiness on the edge of the Agulhas Bank and its relation to frontal features. S. Afr. J. Marine Sci. 14:333-347.

Coetzee, J. 2000. Use of a shoal analysis and patch estimation system (SHAPES) to characterise sardine schools. Aquat. Living Resour. 13(1):1-10.

De Robertis, A., and Higginbottom, I. 2007. A post-processing technique for estimation of signal-to-noise ratio and removal of echosounder background noise. ICES J. Mar. Sci. 64:1282-1291.

De Robertis, A., McKelvey, D.R. and Ressler, P.H. 2010. Development and application of an empirical multifrequency method for backscatter classification. Can. J. Fish. Aquat. Sci. 67:1459-1474.

Dickie, L.M., Dowd, R.G. and Boudreau, P.R. 1983. An echo counting and logging system (ECOLOG) for demersal fish size distributions and densities. Can. J. Fish. Aquat. Sci. 40:487-498.

Dickie, L.M. and Boudreau, P.R. 1987. Comparison of acoustic reflections from spherical objects and fish using a dual-beam echosounder. Can. J. Fish. Aquat. Sci. 44:1915-1921.

Favali, P., Beranzoli, L. and De Santis, A. 2015. Seafloor observatories: A new vision of the earth from the abyss. Springer, Chichester, U.K. 676 pp.

Foote, K.G., Knudsen, H.P. and Vestnes, G. 1987. Calibration of acoustic instruments for fish density estimation: a practical guide. ICES Coop. Res. Rep. 144, ICES, Copenhagen 69 pp.

Foreman, M.G.G., Succhi, D.J., Garver, K.A., Tuele, D., Isaac, J., Grime, T., Guo, M. and Morrison, J. 2012. A circulation model for the Discovery Islands, British Columbia. Atmos. Ocean 50(3):301-316.

Johannesson, K.A. and Mitson, R.B. 1983. Fisheries acoustics: A practical manual for aquatic biomass estimation. FAO Fish. Tech. Paper 240, FAO, Rome, 249 pp.

Kaartvedt, S., Rostad, A., Klevjer, T.A. and Staby, A. 2009. Use of bottom-mounted echo sounders in exploring behavior of mesopelagic fishes. Mar. Ecol. Prog. Ser. 395:109-118.

Lavery, A.C., Wiebe, P.H., Stanton, T.K., Lawson, G.L., Benfield, M.C. and Copley, N. 2007. Determining dominant scatterers of sound in mixed zooplankton populations. J. Acoust. Soc. Am. 122(6):3304-3326.

Mackinson, S. 1999. Variation in structure and distribution of prespawning Pacific herring shoals in two regions of British Columbia. J. Fish Biol. 55, 972-989.

MacLennan, D.N., Magurran, A.E., Pitcher, T.J. and Hollingworth, C.E. 1990. Behavioural determinants of fish target strength. Rapp. P.-V. Réun. Cons. Int. Explor. Mer. 189:245-253.

MacLennan, D.N., Fernandes, P.G. and Dalen, J. (2002). A consistent approach to definitions and symbols in fisheries acoustics. ICES J. Mar. Sci. 59:365-369.

McCarter, B., Hay, D.E., Whither, P. and Kieser, R. 1994. Hydroacoustic herring survey results from Hecate strait, November 22–December 2, 1993. W.E. Ricker Cruise 93HER. Can. Manuscr. Rep. Fish. Aquat. Sci. 2248, 40 p.

Parker-Stetter, S.L., Rudstam, L.G., Sullivan, P.J. and Warner, D.M. 2009. Standard operating procedures for fisheries acoustic surveys in the Great Lakes. Great Lakes Fish. Comm. Spec. Pub. 09-01

Pawlowvicz, R. and McLure, B. 2010. Inverted echosounder for continuous high-resolution water column profiling from the NEPTUNE (Canada) ocean observatory. In: Proceedings of OCEANS 2010, MTS/IEEE Seattle.

Rose, G.A. and Leggett, W.C. 1988. Hydroacoustic signal classification of fish schools by species. Can. J. Fish. Aquat. Sci. 45:597-604.

Sato, M., Dower, J.F., Kunze, E. and Dewey, R. 2013. Second-order seasonal variability in diel vertical migration timing of euphausiids in a coastal inlet. Mar. Ecol. Prog. Ser. 480:39-56.

Sato, M., Horne, J.K., Parker-Stetter, S.L. and Keister, J.E. 2015. Acoustic classification of coexisting taxa in a coastal ecosystem. Fish. Res. 172:130-136.

Simmonds, E.J., Williamson, N.J., Gerlotto, F. and Aglen, A. 1991. Survey design and data-analysis procedures: A comprehensive review of good practice. Int. Counc. Explor. Sea CMB:54, ICES, Copenhagen.

Simmonds, J. and MacLennan, D. 2005. Fisheries acoustics: theory and practice. Second Edition. Blackwell Publishing, London.

Thomson, R.E. and Allen, S.E. 2000. Time series acoustic observations of macrozooplankton diel migration and associated pelagic fish abundance. Can. J. Fish. Aquat. Sci. 57:1919-1931.

Thorpe, S.A. 1986. Measurements with an automatically recording inverted echo sounder; ARIES and the bubbles clouds. J. Phys. Oceanogr. 16:1462-1478.

Trevorrow, M.V., Vagle, S. and Farmer, D.M. 1993. Acoustical measurements of microbubbles within ship wakes. J. Acoust. Soc. Am. 95(4):1922-1930.

Trevorrow, M.V. 2003. Measurements of near-surface bubble plumes in the open ocean with implications for high-frequency sonar performance. J. Acoust. Soc. Am. 114(5):2672-2684.

Vagle, S. and Farmer, D.M. 1992. The measurement of bubble-size distributions by acoustical backscatter. J. Atmos. Oceanic. Tech. 9:630-644.

A Echoview calibration parameters

Coefficients of absorption are calculated using Francois and Garrison's equation (1982). Sound speed, salinity and temperature estimates were derived from a linear fit to the available salinity and temperature data obtained from the CTD casts. In 2015, CTD casts collected by Fisheries and Oceans were used. In 2016, at site 5, CTD data from the Hakai Foundation were used (Hoskyn channel) in addition to DFO's CTD casts, and no interpolation was required for this site.

2015 calibration parameters used in Echoview

Site 1				Absorption coefficient			
Month	Sound speed	Temperature	Salinity	α 67kHz	α 125 kHz	α 200 kHz	α 455 kHz
May	1485.72	10.58	29.28	0.018984	0.03483	0.048577	0.103701
June	1487.74	11.11	29.37	0.019077	0.035483	0.049585	0.104129
July	1489.69	11.63	29.45	0.019148	0.036109	0.050591	0.104638
August	1491.71	12.17	29.53	0.019206	0.036747	0.051658	0.105265
September	1493.72	12.71	29.61	0.019248	0.037375	0.052749	0.105993
Site 2				Absorption coefficient			
Month	Sound speed	Temperature	Salinity	α 67kHz	α 125 kHz	α 200 kHz	α 455 kHz
May	1485.69	10.58	29.28	0.018989	0.03484	0.048589	0.103718
June	1487.71	11.11	29.37	0.019082	0.035492	0.049597	0.104147
July	1489.66	11.63	29.45	0.019154	0.036119	0.050604	0.104656
August	1491.68	12.17	29.53	0.019211	0.036757	0.051671	0.105283
September	1493.7	12.71	29.61	0.019253	0.037385	0.052762	0.106012
Site 3				Absorption coefficient			
Month	Sound speed	Temperature	Salinity	α 67kHz	α 125 kHz	α 200 kHz	α 455 kHz
May	1484.51	10.16	29.69	-	-	0.048415	-
June	1486.41	10.58	30.02	-	-	0.049509	-
July	1488.24	10.98	30.33	-	-	0.050578	-
August	1490.14	11.4	30.65	-	-	0.051725	-
September	1492.04	11.81	30.98	-	-	0.052898	-
Site 4				Absorption coefficient			
Month	Sound speed	Temperature	Salinity	α 67kHz	α 125 kHz	α 200 kHz	α 455 kHz
May	1483.38	9.76	30.07	0.019414	0.034789	0.048231	0.104558
June	1485.13	10.04	30.67	0.019804	0.035676	0.049376	0.105395
July	1486.82	10.31	31.26	0.020185	0.036554	0.050521	0.10627
August	1488.57	10.58	31.86	0.020569	0.037452	0.051703	0.107209
September	1490.31	10.86	32.46	0.020952	0.038373	0.052933	0.108211

2016 calibration parameters used in Echoview

Site 1				Absorption coefficient			
Month	Sound speed	Temperature	Salinity	α 67kHz	α 125 kHz	α 200 kHz	α 455 kHz
May	1485.35	10.51	29.18	0.018919	0.034658	0.048344	0.103539
June	1487.67	11.17	29.11	0.018926	0.035285	0.049375	0.10382
July	1489.86	11.82	29.05	0.018914	0.035893	0.050427	0.104243
August	1492.15	12.48	28.98	0.018874	0.036478	0.051506	0.10479
September	1494.44	13.15	28.91	0.018811	0.037046	0.05262	0.105477
Site 2				Absorption coefficient			
Month	Sound speed	Temperature	Salinity	α 67kHz	α 125 kHz	α 200 kHz	α 455 kHz
May	1486.25	10.51	29.18	0.018774	-	-	-
June	1488.54	11.17	29.11	0.01878	-	-	-
July	1490.76	11.82	29.05	0.018769	-	-	-
August	1493.05	12.48	28.98	0.018729	-	-	-
September	1495.34	13.15	28.91	0.018667	-	-	-
Site 3				Absorption coefficient			
Month	Sound speed	Temperature	Salinity	α 67kHz	α 125 kHz	α 200 kHz	α 455 kHz
May	1484.29	10.07	29.57	0.019097	0.034549	0.048049	0.10384
June	1486.41	10.63	29.66	0.019207	0.035247	0.049093	0.104201
July	1488.45	11.17	29.75	0.0193	0.035917	0.050134	0.104665
August	1490.57	11.72	29.84	0.019378	0.036592	0.051223	0.105244
September	1492.69	11.28	29.93	0.019414	0.036216	0.050546	0.104991
Site 4				Absorption coefficient			
Month	Sound speed	Temperature	Salinity	α 67kHz	α 125 kHz	α 200 kHz	α 455 kHz
May	1483.77	10.05	29.19	-	-	0.047571	-
June	1486.23	10.71	29.24	-	-	0.048719	-
July	1488.62	11.36	29.29	-	-	0.049891	-
August	1491.08	12.03	29.35	-	-	0.051145	-
September	1493.55	12.69	29.4	-	-	0.052403	-
Site 5				Absorption coefficient			
Month	Sound speed	Temperature	Salinity	α 67kHz	α 125 kHz	α 200 kHz	α 455 kHz
May	1485.14	10.57	28.9	0.018772	0.034471	0.048147	0.103247
June	1487.58	11.31	28.73	0.01872	0.03507	0.049182	0.103443
July	1486.54	11.26	28.02	0.018294	0.034302	0.048232	0.102441
August	1487.32	11.05	29.27	0.019027	0.035343	0.049392	0.103999
September	1490.68	12.11	28.97	0.018883	0.036126	0.050867	0.104441